3D Super-Resolution Optical Profiling Using Microsphere Enhanced Mirau Interferometry

Ivan Kassamakov[1], Sylvain Lecler[2], Anton Nolvi[1], Audrey Leong-Hoï[2], Paul Montgomery[2] and Edward Hæggström[1]

[1] *University of Helsinki, Helsinki, Finland.*
[2] *ICube Laboratory, University of Strasbourg-CNRS, Strasbourg, France.*

Corresponding author e-mail address: ivan.kassamakov@helsinki.fi

We present quantitative three dimensional images of grooves on a writable Blu-ray Disc based on a single objective Mirau type interferometric microscope, enhanced with a microsphere which is considered as a photonic nanojet source. Along the optical axis the resolution of this photonic jet interferometry (PNI) based system is a few nanometers while the lateral is a better than 100 nm. To understand the physical phenomena involved in this kind of imaging we have modelled the interaction between the photonic jet and the complex disc surface. Agreement between simulation and experimental results is demonstrated. We underline that the ability of the microsphere to generate a photonic nanojet can be used to understand its role in imaging. The potential role of coherence in the super-resolution explanation is illustrated. The presented modality may have a large impact on many fields from bio-medicine to nanotechnology.

Introduction

Bio-imaging, especially label-free bio-imaging, is globally large and rapidly growing both academically and commercially. Primary trends are three dimensional (3D) imaging, super-resolution imaging (Nobel Prize for Chemistry 2014)[1] label-free imaging (no fluorophores, dyes or nanomarkers), quantitative (metrologically traceable) imaging, high-throughput imaging (currently hundreds of samples per microscope per day), and fresh sample imaging (little or no sample preparation). We address the first three issues. Our approach is to use a single objective Mirau type interferometric microscopy enhanced with a microsphere that is considered as a photonic nanojet lens to achieve super-resolved and quantified 3D label-free imaging.

The wave nature of light limits the 3D resolution in classical optical microscopy[2,3]. The diffraction limit applies to far-field imaging where the specimen is many thousands of wavelengths from the objective. Super-resolution techniques create images with higher resolution than the Abbe limit[4] [4]. Many such modalities exist[5–7] but these techniques require labelling agents. Near-field optical techniques are label-free, but they are limited to surface and near surface imaging[8]. One of the few 3D label-free techniques is tomographic diffractive microscopy (TDM) that achieves super-resolution using a synthetic numerical aperture[9], giving a typical resolution limited to λ/4.

Interference microscopy, including phase shifting microscopy and coherence scanning interferometry (a.k.a scanning white light interferometry, SWLI), is a mature non-contact technique that provides quantitative information across large areas with a sub-nanometer axial resolution[2,10]. The technique is able to resolve and measure closely spaced 3D details such as nanometric surface roughness and even atomic step heights as long as the lateral details of the features can be resolved. But because the method is laterally diffraction limited, this means that features laterally smaller than the diffraction limit cannot be measured. The ability to overcome this limitation is demonstrated in this paper using a single objective Mirau type interferometric microscope enhanced with a photonic nanojet lens.

A photonic nanojet is a narrow light beam situated near the shadow-side surface of an illuminated dielectric microsphere whose diameter is a few wavelengths of the light source[11,12]. The nanojet exhibits: (1) high

intensity (100x the incident power density); (2) subdiffraction beam width; (3) several wavelengths long reach. We show how the ability of the microsphere to generate a photonic nanojet can be used to understand these imaging properties

Results

Recently, lateral super-resolution has been achieved using nanolenses, microdroplets, and microspheres placed on the sample, below the microscope objective[13]. Silica (n = 1.46) with Ø = 2–9 µm, and barium titanate microspheres (n = 1.9) with Ø = 100 µm have provided images of recordable Blu-ray Disc line structures, nanopores, and adenoviruses[14,15]. The lateral resolution of the systems was < 100 nm. It is unclear exactly how this microsphere approach works[13–15] since the sub-diffraction width (around λ/3) of the photonic nanojet cannot by itself explain super-resolution. Potentially super-resolution is achieved by looking "through the microsphere" at a virtual image produced by the microsphere[13]. The existence of this virtual plane can be justified based on the simulation of the nanojet. By considering the microsphere as a photonic jet lens, the imaging properties can be investigated numerically. We present such a study in the following section.

Simulations

Light is scattered by a microsphere in the far field, but can be concentrated in its vicinity. By analogy, this concentration which is known as the photonic nanojet, can be considered as the microsphere focus. The photonic jet created by a microsphere (Ø = 11 µm, n=1.68) illuminated by a white light incident plane wave, has been computed (Fig. 1). The maximum intensity of the photonic nanojet is 0.5 µm below the bead (along y), is 2 µm long (FWHM along the y direction), and has a FWHM of 0.5 µm (along the x direction). By analogy with an imaging lens, since the nanojet is outside the microsphere, an object between the microsphere and the photonic jet may be magnified in a virtual image plane. Beyond this analogy the studies of the photonic nanojet have shown that the microspheres do not obey the laws of geometrical optics and that rigorous electromagnetic methods are required[11,12].

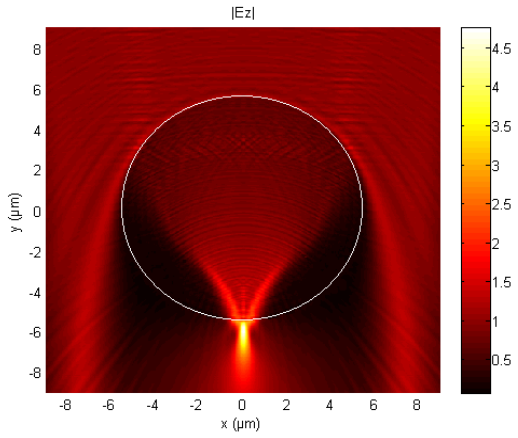

Figure 1. *Photonic nanojet generation resulting from unitary (1 V/m) plane waves (λ from 400 nm to 1000 nm) illuminating (from the top) an 11 µm microsphere (n = 1.68) using 2D TE FEM electric field simulation (absolute values $|E_z|$)*

We have investigated the "virtual plane" hypothesis. To determine the position of this virtual image plane, we first simulated two point sources A and A' in the sample plane (emitting at λ=600 nm), separated by 300 nm (Fig. 2a). The wavefront emerging from the top of the bead (Ø = 11 µm, n=1.68) is curved. Since the centre of this wavefront gives the approximate position of the virtual image plane, this plane can now be found by time-reversal propagation of the wavefront from [B, B'] (Fig. 2a), without the bead.

The results when A and A' are in phase are shown in Fig. 2b where the dashed sphere indicates the initial position of the sphere. The virtual images of the two point sources appear as overlapping diffraction patterns situated at the maximum of the central intensity along *y* (dashed line at *y* = -25 µm in Fig. 2b). The depth of field extends 5 µm to either side of the point of maximum intensity. While the virtual image position is found, justifying the photonic jet lens concept, the two point sources are not resolved.

Concerning super-resolution, one hypothesis, yet to be confirmed, is that the microsphere converts the high frequency spatial components of the evanescent field into propagating modes that allow far-field imaging of sub-diffraction-limited sample features[15]. In addition to this idea, the role of the coherence of the illumination should be accounted for when trying to explain the physics of microsphere-assisted super-resolution[16]. We have also investigated this hypothesis by repeating the simulations with the two point sources A and A' being out of phase. The virtual images conveyed by the two diffraction patterns can be distinguished at the same position (dashed line at *y* = -25 µm in Fig. 2c). The two intensity maxima are now separated along *x* by 2 µm. The two points are resolved, corresponding to a lateral magnification of x6 (2 µm/0.300 µm). This result indicates that the phase may be involved in super-resolution. Thus, microsphere-assisted imaging could provide lateral super-resolution and the phase could concurrently be exploited to quantify the third dimension leading to photonic nanojet interferometry (PNI).

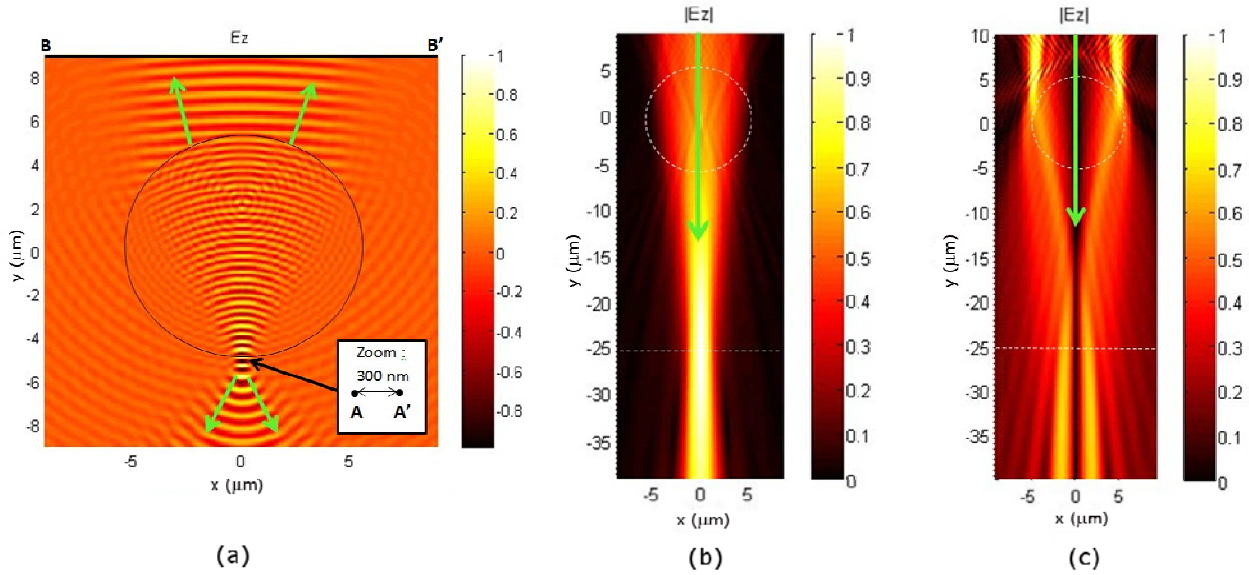

Figure 2. *Attempts to predict the performance of the microsphere assisted interferometric microscope. The virtual image plane positions (dashed lines) are determined using 2D FEM simulations for an 11 µm microsphere (n = 1.68) and λ = 600 nm light. The arrows indicate the direction of light propagation. (**a**) Electric field (real part) propagation from two point sources A and A' that are in phase, separated by 300 nm, and positioned below the microsphere in the plane at y = -5.5 µm. (**b**) Time-reversal propagation, without the sphere, of the wavefront emanating from [B, B'] in (a) (absolute values $|E_z|$). The virtual image plane is 20 µm below the bead. (**c**) As in (b) when the two sources A and A' in (a) are out of phase*

Experimental setup

We designed an experiment to show that microsphere-assisted interference microscopy provides label-free nano-3D imaging[17]. To increase the lateral resolution of our custom-built SWLI system we placed polymer spheres (melamine formaldehyde, Corpuscular Inc., Ø = 11 µm, n = 1.68) above the Blu-ray Disc (Verbatim BD-R, Datalife)[18,19] surface by self-assembly[13]. The single lens system uses a Mirau-type interferometric objective (Nikon x50, *NA* = 0.55) with white light illumination (halogen lamp - Philips 7724, 12 V, 100 W) centred at λ=600 nm, which under normal conditions gives a classical lateral resolution of 0.67 µm. The images

were acquired using a high-sensitivity, small pixel size, black and white CMOS camera (Hamamatsu ORCA-Flash 2.8) (Fig. 3).

The surface features of a recordable Blu-ray Disc whose protective polymer layer had been removed were also measured by SEM (Hitachi S-4800 FESEM) with 2.5 nm lateral resolution[20] which was calibrated using a SIRA SEM calibration specimen S170[21] and by a metrological AFM system[22]. For SEM imaging, the disc surface was covered with a 4 nm thick gold layer. Care was taken to limit the electron beam power to avoid altering the disc surface.

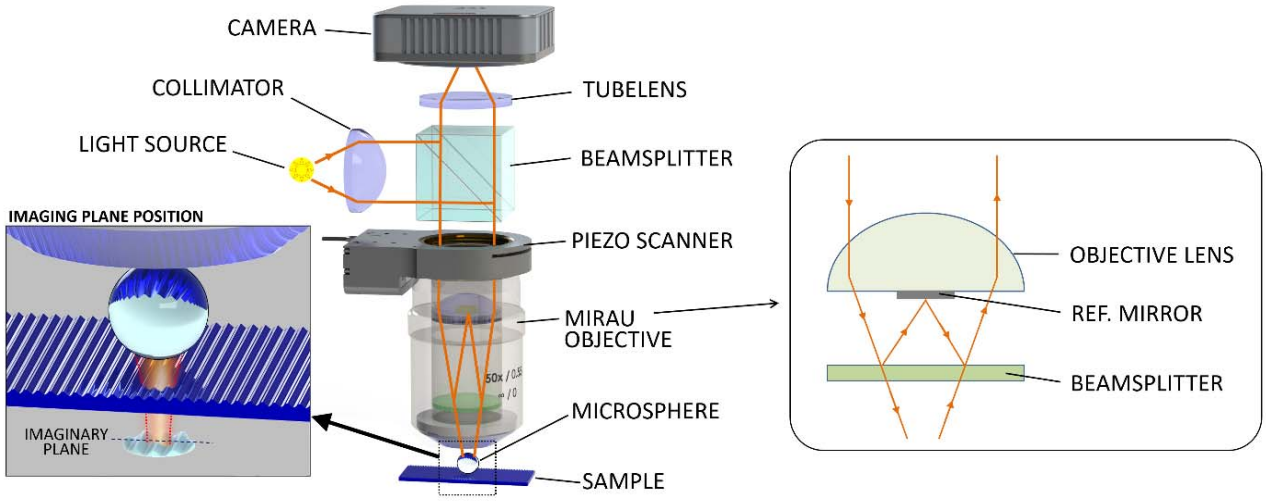

Figure 3. *Microsphere-assisted imaging: setup with a Mirau type interferometer and a microsphere placed on top of/above an object. The sphere projects a virtual image into the far-field that is collected by the objective lens. Zoom-in is not to scale. The insert on the right shows the design and the ray propagation in a single objective Mirau type interferometer.*

Simulation and Experimental results

To predict the expected super-resolved image we repeated the simulation procedure described earlier for the entire spectral range of the instrument. The two point sources were replaced by the Blu-ray Disc, illuminated by a plane wave passing through the Ø=11 µm microsphere. The disc is a complex structure[23]. We approximated its surface by a multilayer rectangular grating with a 320 nm period made of a polycarbonate substrate (n_{PC} = 1.55), a 100 nm thick silver reflective layer, and a 25 nm thick SiO_2 dielectric layer (n_{SiO2}=1.5), see Fig. 4b. The light dispersion by silver was accounted for[24]. For time-reversal propagation of the wave reflected by the sample (Fig. 4a,b), the localization of the virtual image plane is not so obvious since several maxima are visible, but the plane is at the position predicted in Fig. 2b and Fig. 2c (20 µm below the sphere, plane at y = -25 µm).

Our experiments partly validate the simulation predictions. Figure 5a shows the results of an experimental PNI measurement of the Blu-ray Disc surface. A 3D structure is observed where the 323 ±2.5 nm inter-groove distance and 112 ±2.5 nm wide grooves are resolved (Fig. 5a). The SEM image in Fig. 5a gives an indication of the line spacing. The 2D image through the sphere is shown in Fig. 5b, while the non-corrected 3D image with aberrations measured by PNI is depicted in Fig. 5c. This demonstrates a near 6-fold increase in lateral resolution compared to measurements made with the Mirau objective alone. Indeed, without the microsphere, the grooves can neither be observed nor measured with the classical interferometric system. The groove depth measured by AFM is 21.0 – 24.8 nm (Fig. 5d).

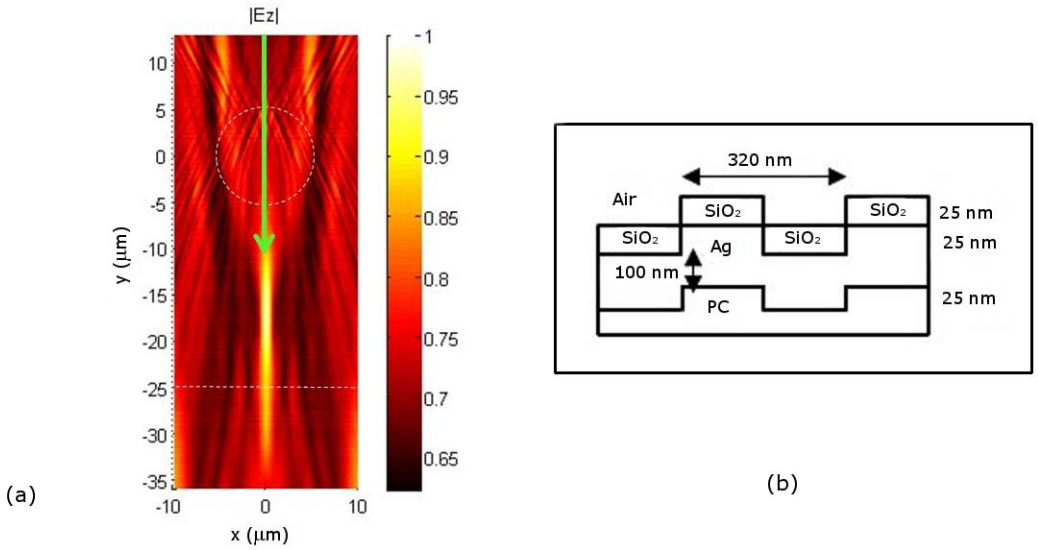

Figure 4. *Simulation of instrument interaction with the Blue-ray Disc (**a**). Determining the position of the virtual image (dashed line) plane using 2D FEM simulation, absolute electric field $|E_z|$. The first interaction (not represented) of a plane wave with the 11 µm sphere and the Blu-ray Disc (see (**b**) for the Blu-ray Disc model) allows the calculation of the outgoing wave which is then time-reversed and propagated without the sphere. The arrow indicates the direction of light propagation.*

Aberrations corrected image is presented on Fig. 6a.The resolved grooves are 17.2 – 23.8 nm deep. The designed trapezoidal shape of the disc grooves can be found in[23], together with the exact angles of the slope. The same shape is depicted in[18] and has been measured in[19]. The results obtained (Fig. 5d and Fig. 6b) show a close to sinusoidal shape resembling that published in[26]. In our opinion this is because of the remains from the disc protective layer.

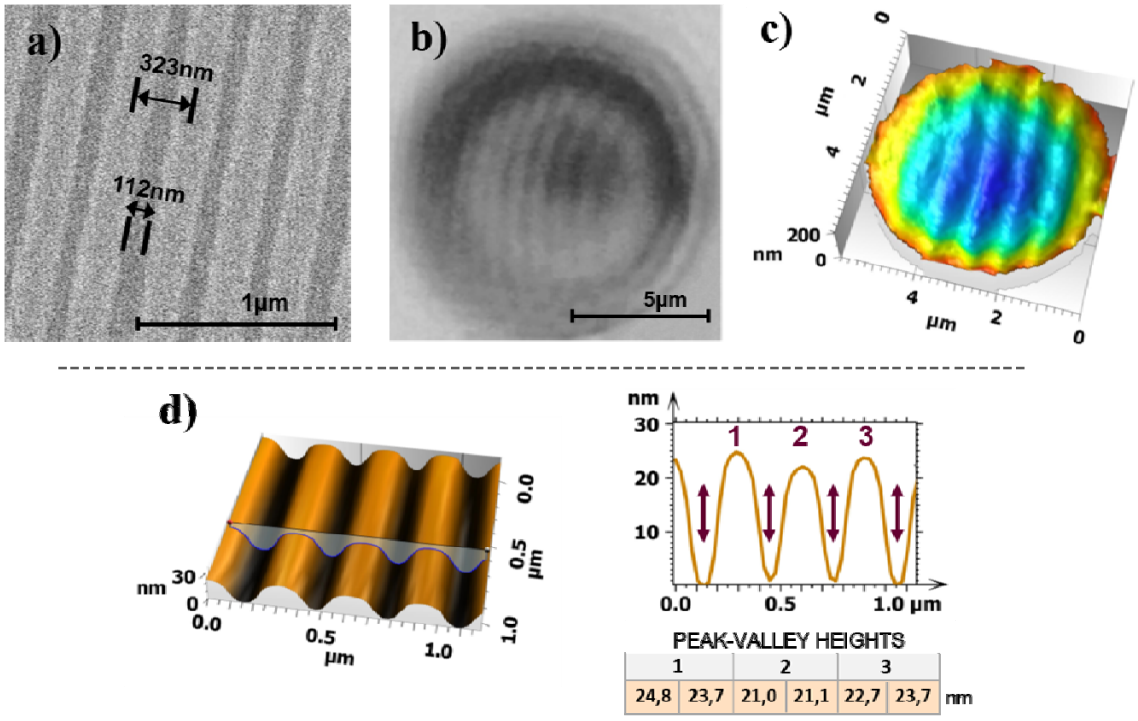

Figure 5. *Blu-ray Disc: (**a**) SEM image and a groove measurement. (**b**) 2D image through sphere. (**c**) Uncorrected 3D image with aberrations measured by PNI. (**d**) AFM 3D and cross sectional profile showing resolved grooves 21.0 – 24.8 nm deep.*

Discussions

Super-resolution has been achieved. Our results show the ability to improve the lateral resolution of a single-lens far field interferometric microscope using a photonic jet lens, so considerably extending the performance in terms of imaging and measuring 3D nanometric surface roughness and structures. The experimental results demonstrate a lateral resolution of better than 100 nm and an axial measurement resolution of several nanometers. The simulations confirm the possibility of improving the lateral resolution of 3D measurements compared to classical far-field imaging and suggest that the phase change of the reflected wave plays a major role in nanoresolution imaging.

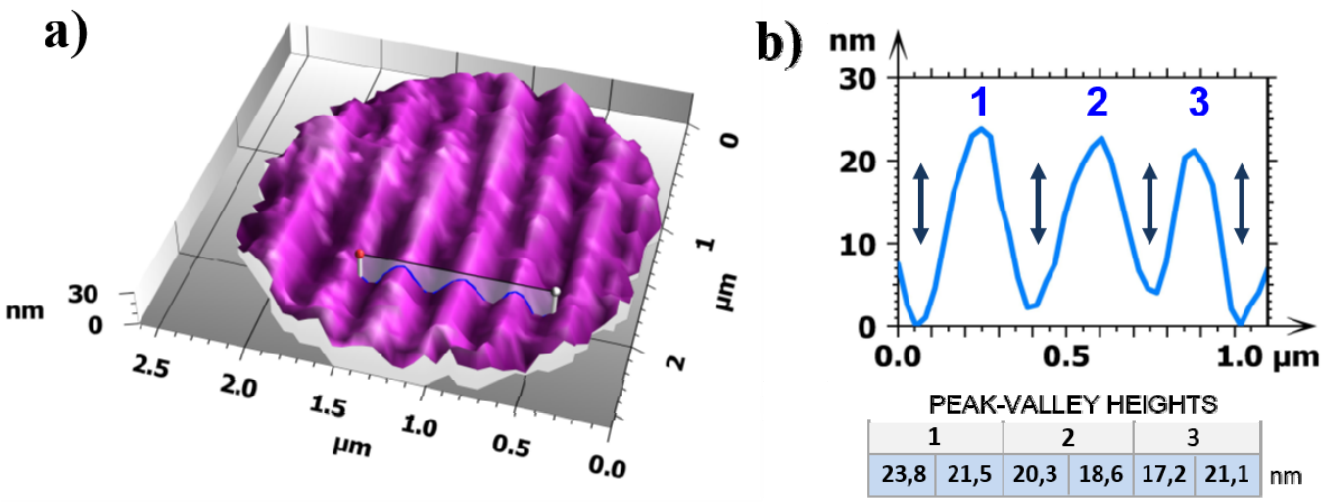

Figure 6. *Blu-ray Disc: **(a)** 3D image measured by PNI. **(b)** Cross sectional profile from position indicated in (a), showing resolved grooves 17.2 – 23.8 nm deep.*

Finding a suitable polymer sample featuring known X, Y, Z nanometer dimensions was difficult. Having chosen the Blu-ray Disc, a challenge was to remove the cover layer without damaging the layer structure, which could change the measurement results compared with the design specifications. Furthermore, residues from the removed layer could remain and affect the measured profile. The slight difference in the measured heights using PNI and AFM could be due to the self-assembly procedure not allowing exact positioning of the spheres, or because of slightly different measurement areas being analyzed by each microscope.

The physics of super-resolution imaging is still unclear. The experiments verified that the depth of focus of the objective was extended by the photonic jet, but not fully confirmed the simulation prediction that the jet also increases the magnification of the objective in the volume of focus. These predictions are shown in the single wavelength simulation (Fig. 2b,c). To further explore these exciting results, more realistic simulations need to be performed that take into account the wall angle and the properties of the phase changing material as described in [23]. Such simulations would probably not dramatically change the predictions but could provide a better understanding of the physical phenomena involved in the imaging.

An alternative explanation of the difference in magnification between the results of simulation and experiment may come from considering the interference conditions. By adding the microsphere, the optical path length in the sample arm is increased, which unbalances the two arms of the interferometer which normally need to be within the coherence length of the light source (in this case, FWHM = 1.2 µm) to produce interference. In the presence of a planar glass layer in the sample arm, what is known as the coherence gate would be separated from the focal gate, so preventing interference[25]. However, for a small diameter bead (11 µm), the two gates still overlap sufficiently along the optical axis because the focal gate is also displaced by the microsphere (in the same direction) to allow the interference fringes to be made visible. Moreover, the experimental results show

that the depth of focus of the Mirau objective is increased beyond the value of 0.9 μm in air, possibly due to the effect of the photonic nanojet (PNJ). This finding supports the notion that the role of the PNJ may be significant. In addition, the fact that the path length difference cannot be modified in the Mirau objective used, means that the optimum focus probably cannot be attained. As a consequence the magnification is merely ~x2.6.

During the preparation of this article a Linnik interferometer system featuring two matched lenses was published[26]. These results confirm that super-resolution imaging is not confined to Mirau systems.

Briefly, super-resolution imaging works but it is yet unclear why. These results may signal the beginning of a new era in quantified 3D surface and sub-surface imaging with applications ranging from malaria screening to the quality assurance of integrated microelectronic circuits.

Methods

The electromagnetic simulations were performed with a 2D finite element method (FEM) that solves the vectorial propagation equation. TE waves were considered, in which the electric field is orthogonal to the plane studied). The source was introduced on a scattering boundary condition. Perfectly matched layer (PML) absorbing boundary conditions were used for all other boundaries. The space was meshed with a Delaunay triangulation in which the elements are smaller than $\lambda/10$. For white light, the spectral range of the source was accounted for by incoherently summing simulations run for wavelengths from 400 nm to 1000 nm (in 50 nm steps).

To make the high resolution measurements, the sample was scanned along the optical axis while imaging it through the microsphere. The axial scan range was selected to cover all the interference patterns produced by the sphere, limiting the scan to a range of 20 μm. Custom made data acquisition software was used to scan through the range with 68.75 nm steps[27] taking 8 times averaged pictures for each height position. From the set of images obtained, the interference data was analysed at each pixel in terms of the light intensity as a function of the relative height. By applying the algorithm from Harasaki *et al.*[27] an accurate surface position map for every pixel was calculated, so producing a 3D data map. This data was then analysed with commercial software[28] to extract geometrical values and to produce a 3D view. Since the microsphere adds magnification to that provided by the objective, the lateral scale of the measured 3D data was corrected by using a magnification factor calculated from the ratio between the measured pitch to the nominal pitch retrieved from the literature[18,19].

The data acquisition times for scanning through the 20 μm range with 8 time averaged images at each step is a couple of minutes. The scanning time depends on the axial range, the camera frame rate (48 fps in our case), and the averaging. With our system, for a maximum range of 100 μm, the scanning time is from 20 seconds to a few minutes, depending on the acquisition parameters."

The 323 ±2.5 nm inter-groove distance (Fig. 5c) was determined from SEM measurements and the associated calibrated values of the pixel size in the SEM data file. The inter-groove distance was calculated by counting the number of pixels between two points and then multiplying this by the pixel size.

References

1. Ehrenberg, M. Super-resolved fluorescence microscopy. *The Royal Swedish Academy of Sciences*, Stockholm, Sweden (2014).

2. de Groot, P. Principles of interference microscopy for the measurement of surface topography. *Advances in Optics and Photonics*, **7**, 1 (2015).

3. Mansfield, S. M. & Kino, G. S. Solid immersion microscope. *Appl. Phys. Lett.* **57**, 2615-2616 (1990).

4. Neice, A. Methods and Limitations of Subwavelength Imaging. *Adv. in Imag. and El. Phys.* **163**, 117–140 (2010).

5. Klar, T.A., Jakobs, S., Dyba, M., Egner, A. & Hell S.W. Fluorescence microscopy with diffraction resolution barrier broken by stimulated emission. *Proc. Natl. Acad. Sci.*, USA, **97,** 8206-8210 (2000).

6. Betzig, E. *et al.* Imaging intracellular fluorescent proteins at nanometer resolution. *Science* **313,** 1642-1645 (2006).

7. Rust, M. J., Bates, M. & Zhuang, X. Subdiffraction-limit imaging by stochastic optical reconstruction microscopy (STORM). Nature Methods **3,** 793–795 (2006)

8. Fillard, J.P. Near Field Optics and Nanoscopy. *World Scientific*, Singapore, 197-214 (1996).

9. Haeberlé, O., Belkebir, K., Giovaninni, H. & Sentenac, A. Tomographic Diffractive Microscopy: Basics, Techniques and Perspectives. *J. Mod. Opt.* **57**, 686-699 (2010).

10. Malacara, D. *Optical Shop Testing* 3th edn. (John Wiley & Sons, 2007).

11. Chen, Z., Taflove, A. & Backman, V. Photonic nanojet enhancement of backscattering of light by nanoparticles: a potential novel visible-light ultramicroscopy technique. *Opt. Expr.* **12**, 1214-1220 (2004).

12. Lecler, S., Takakura, Y. & Meyrueis, P. Properties of a three-dimensional photonic jet. *Opt. Lett*. **30**, 2641-2643 (2005).

13. Wang, Z. *et al.* Optical virtual imaging at 50 nm lateral resolution with a white-light nanoscope. *Nature Comm*. **2**,218 doi: 10.1038/ncomms1211 (2011).

14. Darafsheh, A., Walsh, G. F., Dal Negro, L. & Astratov, V.N. Optical super-resolution by high-index liquid-immersed microspheres. *Appl. Phys. Lett.* **101**, 141128, (2012).

15. Li, L., Guo, W., Yan, Y., Lee, S. & Wang, T. Label-free super-resolution imaging of adenoviruses by submerged microsphere optical nanoscopy. *Light: Sci. & Appl.* **2,** e104; doi:10.1038/lsa.2013.60 (2013).

16. Maslov, A. V. & Astratov, V. N. Imaging of sub-wavelength structures radiating coherently near microspheres. *Appl. Phys. Lett.* **108**, 051104 (2016).

17. Kassamakov I, Hæggström E, inventors; University of Helsinki, assignee. Arrangement and method of determining properties of a surface and subsurface structures, International patent application PCT/FI2015/050876, 2015 Dec 11.

18. Lin, S. K., Lin, I. C. & Tsai, D. P. Characterization of nano recorded marks at different writing strategies on phase-change recording layer of optical disks. *Opt. Expr*. **14**, 4452-4458 (2006).

19. White paper Blu-ray Disc format 4th edition, 2015. http://blu‑raydisc.com/ (2015).

20. Kemell, M. Short instructions for use. Hitachi S-4800 FESEM, Version 4 (2008).

21. Van Loenen Instruments, Zaandam, The Netherlands, http://www.loeneninstruments.com (2014).

22. Korpelainen, V., Seppä, J. & Lassila, A. Design and characterization of MIKES metrological atomic force microscope. *Precis. Eng.* **34 (**4), 735-744 (2010).

23. Brusche, J.H., Segal1, A. & Vuik, C. An efficient numerical method for solid–liquid transitions in optical rewritable recording. *Int. J. Numer. Meth. Engng.* **77,** 702-718 (2009).

24. Palik, E. D. *Handbook of optical constants of solids* (Elsevier, 1997).

25. Federici, A., Costa, H. S. G. da, Ogien, J., Ellerbee, A. K. & Dubois, A. Wide-field, full-field optical coherence microscopy for high-axial-resolution phase and amplitude imaging. *Appl. Opt.* **54,** 8212–8220 (2015).

26. Wang, F. *et al.* Three-Dimensional Super-Resolution Morphology by Near-Field Assisted White-Light Interferometry. *Sci. Rep.* **6**, 24703; doi: 10.1038/srep24703 (2016).

27. Harasaki, A., Schmit, J. & Wyant, J. C. Improved vertical scanning interferometry. *Appl. Opt*. **39**, 2107–15 (2000).

28. MountainsMap 7.3, Digital Surf (http://www.digitalsurf.com/brochures/DigitalSurf_EN.pdf)

Author contributions

I.K. conceived the basic idea and designed the experiments, I.K. and E.H. designed the optical system and the experiments, A.N. carried out the experiments under supervision of I.K. and E.H. S.L. performed the simulations. A.L.H. and P.M. together with other authors analysed the experimental results and contributed to the discussions and interpretations. I.K. wrote the manuscript, with input from all the authors.

Additional information

Supplementary information is available in the online version of the paper. Reprints and permissions information is available online at www.nature.com/reprints. Correspondence and requests for materials should be addressed to I.K.

Competing financial interests

The authors declare no competing financial interests.

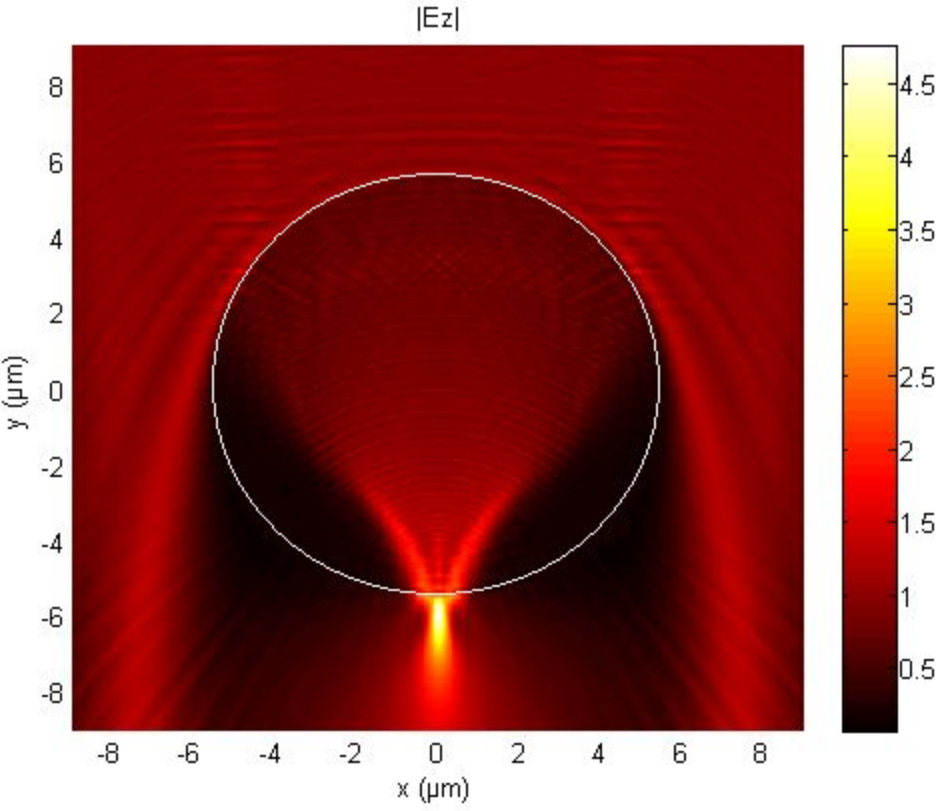
|Ez|
y (μm)
x (μm)
8
6
4
2
0
-2
-4
-6
-8
-8
-6
-4
-2
0
2
4
6
8
4.5
4
3.5
3
2.5
2
1.5
1
0.5

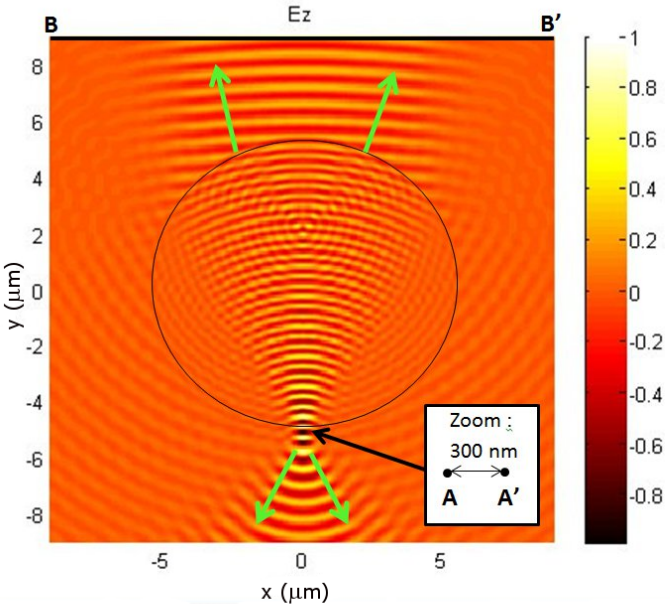

(a)

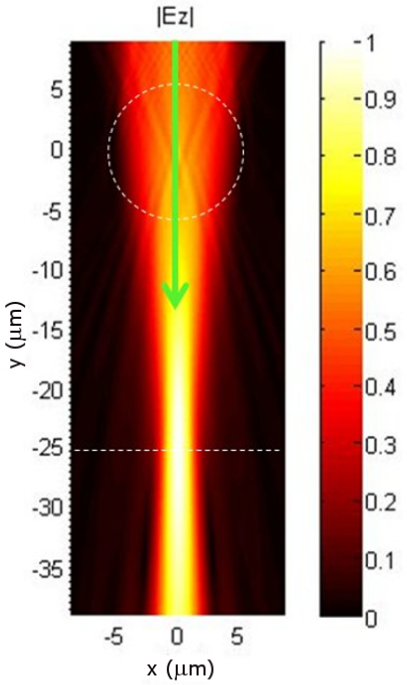

(b)

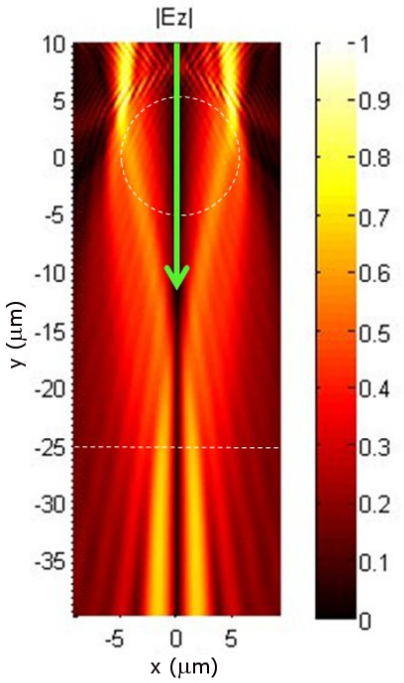

(c)

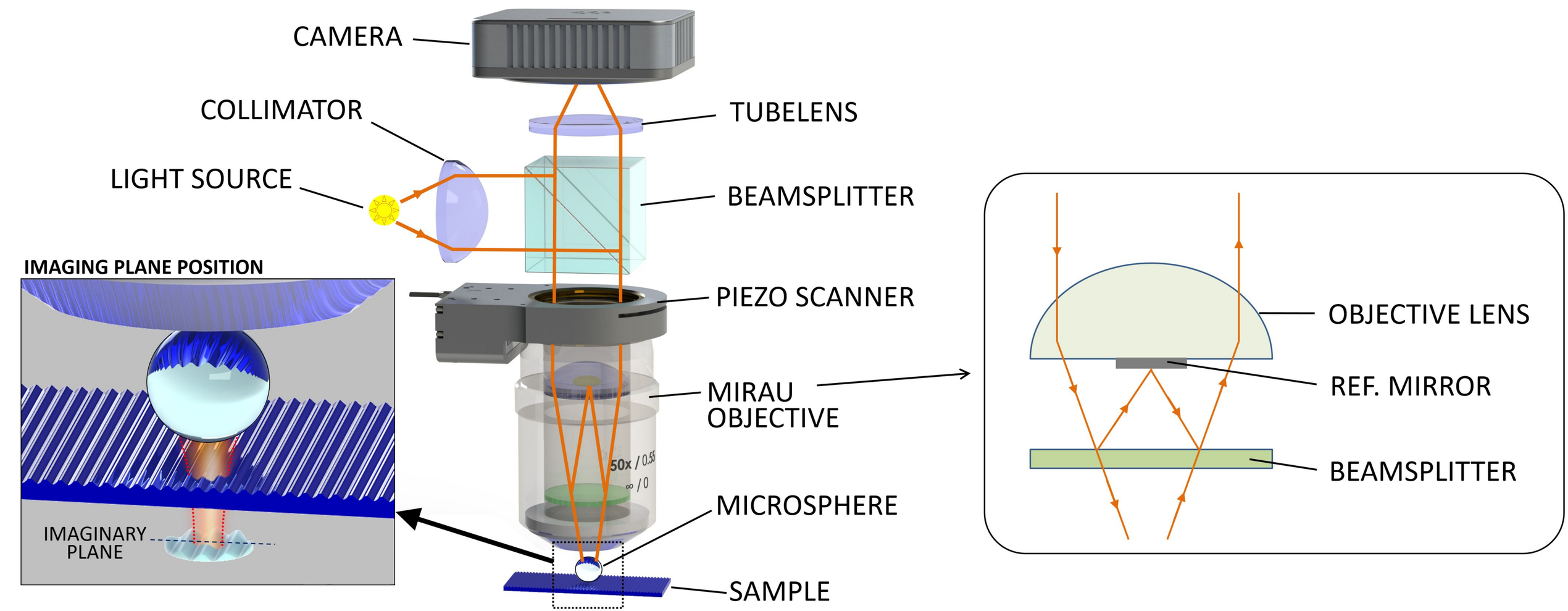
CAMERA
COLLIMATOR
LIGHT SOURCE
TUBELENS
BEAMSPLITTER
PIEZO SCANNER
MIRAU OBJECTIVE
MICROSPHERE
SAMPLE
IMAGING PLANE POSITION
IMAGINARY PLANE
OBJECTIVE LENS
REF. MIRROR
BEAMSPLITTER

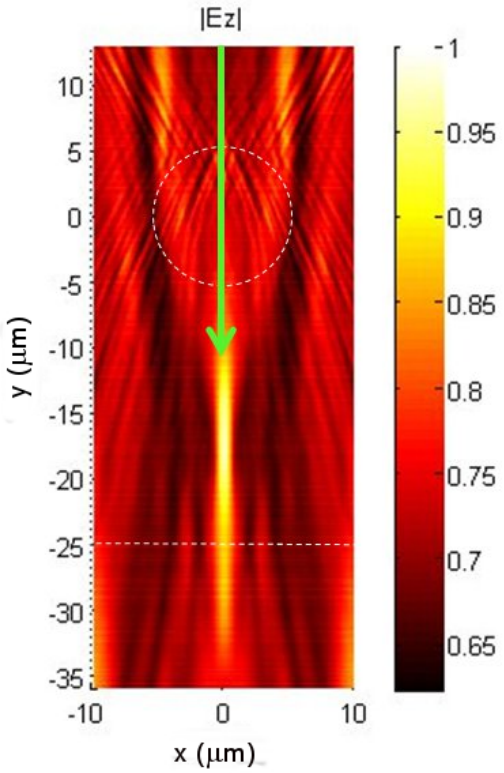
|Ez|
10
5
0
-5
-10
-15
-20
-25
-30
-35
y (μm)
-10
0
10
x (μm)
1
0.95
0.9
0.85
0.8
0.75
0.7
0.65

(a)

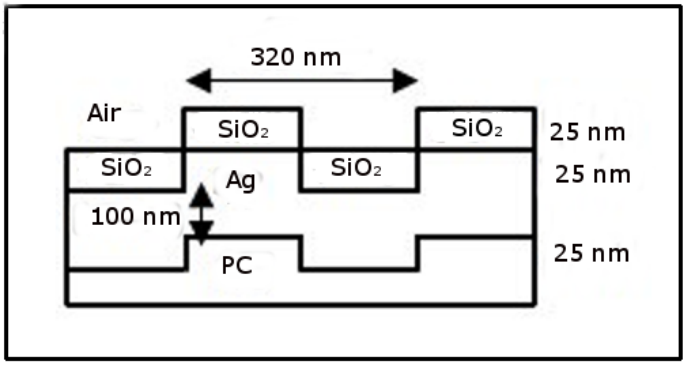
320 nm
Air
SiO2
SiO2
SiO2
SiO2
Ag
100 nm
PC
25 nm
25 nm
25 nm

(b)

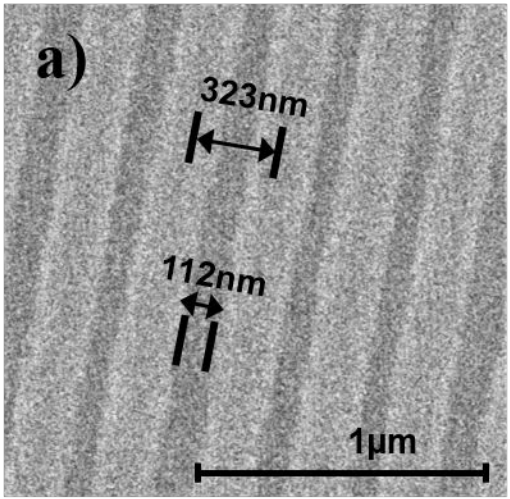

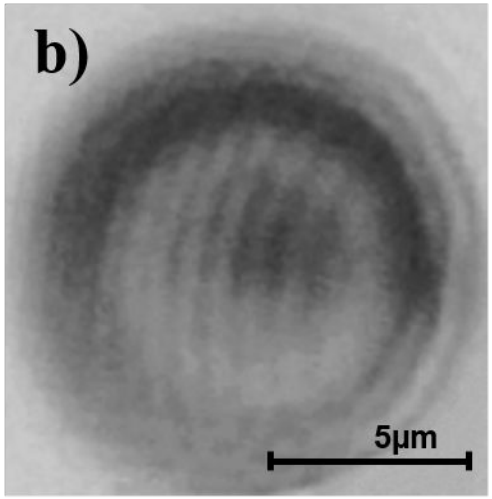

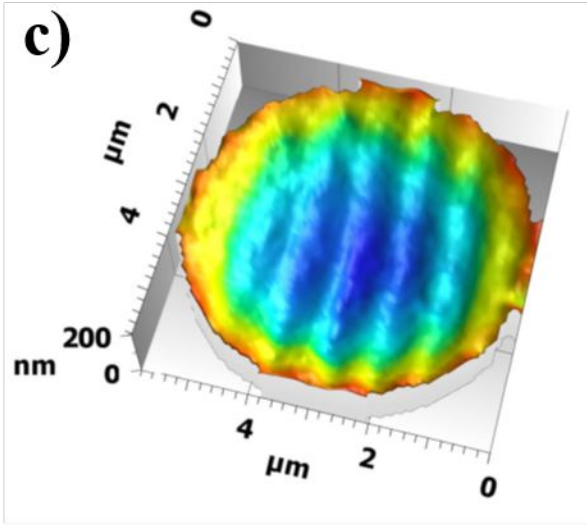

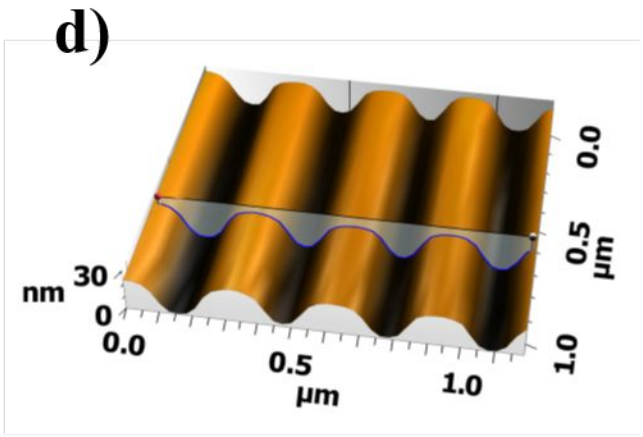

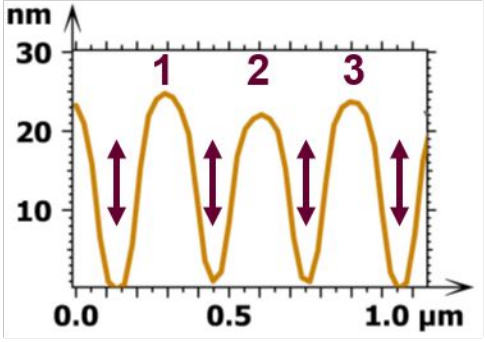

PEAK-VALLEY HEIGHTS

1		2		3		
24,8	23,7	21,0	21,1	22,7	23,7	nm

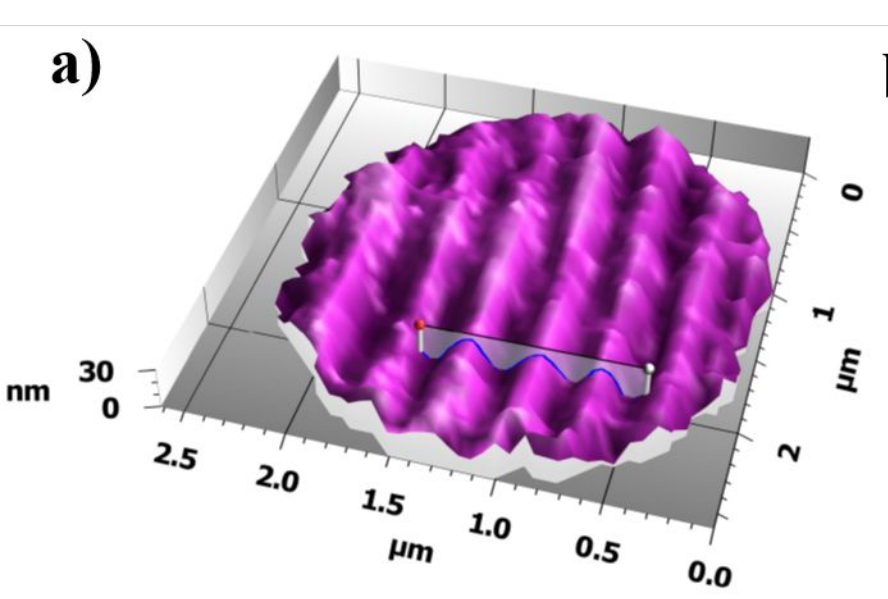

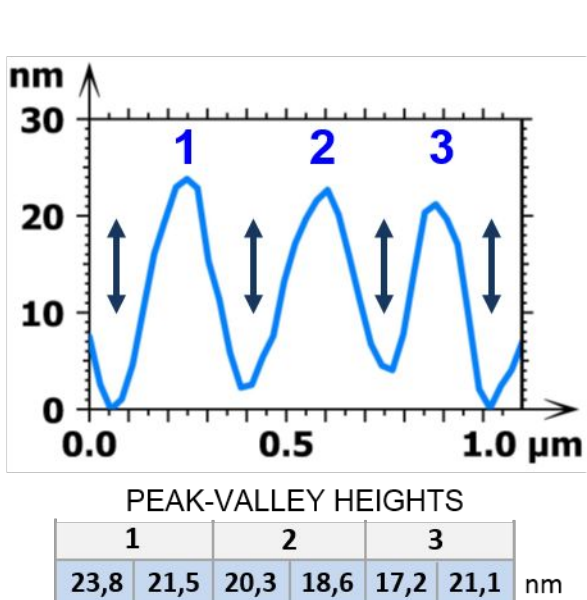

PEAK-VALLEY HEIGHTS

1		2		3		
23,8	21,5	20,3	18,6	17,2	21,1	nm